2015 IEEE Conference on Control Applications (CCA)
Part of 2015 IEEE Multi-Conference on Systems and Control
September 21-23, 2015. Sydney, Australia

Opto-Acoustic Distance Measurement Using Spread Spectrum Techniques and Carrier Phase Measurements

Philipp Rapp, Oliver Sawodny, and Cristina Tarín

Abstract— **In this contribution, a novel opto-acoustic indoor navigation system for linear distance measurement is presented. The novelty consists in the simultaneous use of envelope time-of-flight (ETF) and carrier phase (CPH) measurements. In particular, we establish a two-channel link consisting of an ultrasound and infrared channel, the latter using a carrier frequency equal to the ultrasound frequency. In order to render the system extendible for multiple transmitters and receivers, code-division-multiple-access using Gold codes is employed, as all ultrasound and infrared signals share the same carrier frequency. This is also beneficial for multipath scattering suppression. The time difference between the carrier phase of the received ultrasound and infrared signals offers a high resolution but ambiguous distance signal. On the other hand, correlation of the received signals yields a coarse but unique distance signal. Experimental results show that a measurement resolution in the submillimeter range is feasible.**

I. Introduction

Satellite-based navigation methods like, e. g., Navstar GPS, are well-researched and the navigation solutions are available to the public. However, this is not the case for indoor navigation, where equally efficient solutions are still sought. A comprehensive overview can be found in [1]. Indoor navigation is commonly addressed as positioning when only insufficient or no satellite coverage is available. Examples include large public office buildings (airports, hospitals, museums, train stations, campuses) and private locations (shopping malls, conference sites, urban areas), but also industrial robot manipulation or even medical robotics with applications ranging from logistics and security over health and family care up to emergency and rescue.

The industry already provides several dedicated solutions based on different technologies: Optical positioning is currently becoming a dominating technique as can be observed from the advance of commercially available systems (see [2], [3]). This is due to the improvement and miniaturization of cameras together with the increase in data transmission rates and the development of image processing algorithms. These camera-based system architectures mostly rely on triangulation to reconstruct a 3D motion through 2D observations of the sensors (cameras). The main drawback of optical systems is that they require line-of-sight between transmitter and receiver. Furthermore, their high cost prohibits a large distribution.

In contrast to optical systems, radiofrequency (RF) positioning systems are more robust with respect to shadowing (i. e., loss of the line-of-sight). This depends however on the technology being employed. Triangulation and fingerprint techniques are mainly used [4], [5]. Depending on the required transmission rate, the RF band must be selected. Although these RF systems provide good localization accuracy, the deployed devices are costly and heavy.

Acoustic sensors are widely used for perception of the environment in many robotic applications due to their success in combining cost efficiency, processing time, and accuracy [6], [7], [8].

Ultrasound signals together with time-of-arrival (TOA) techniques are used in most acoustical systems. In the MIT cricket system [9], the positions are estimated through triangulation and RF signals are used for the synchronization of TOA measurements. Ultrasound signals based on binary phase shift keying modulated spreading codes are used in [10] and a fingerprinting approach is presented in [11]. As many acoustic systems suffer from ambient noise that shall be suppressed, several techniques have been presented regarding this issue [12], [13].

Most acoustic systems only send sound pings, making them error-prone with respect to multipath propagation. Moreover, it is not possible to distinguish individual transmitters, because homogeneous pings cannot be distinguished without additional timing or infrastructure elements being added.

This results in the need to use encoding schemes such as, e. g., time division multiplex (TDM) or frequency division multiplex (FDM). Those have several drawbacks: TDM is not only difficult in synchronization, but reduces the sampling frequency of the distance signal. FDM requires the use of several distinct carrier frequencies, which in turn requires the system to provide several distinct transducers (each with its own resonance frequency), making it more complex and expensive.

In the present contribution we propose an opto-acoustic system for linear distance measurement that combines code-division-multiple-access (CDMA)-based time-of-flight (TOF) of the envelope as well as carrier phase measurements. The first mode is called ETF (**E**nvelope **T**ime-of-**F**light), whereas the second mode is called CPH (**C**arrier **Ph**ase measurement). The benefit of CDMA is that a large number of transmitters can work simultaneously, which results in a high sampling frequency of the distance signal. Moreover, the large number of transmitters ensures that at least three of them are visible at all times, allowing tri- oder multilateration.

This linear distance measurement is the basis for a mul-

P. Rapp (rapp@isys.uni-stuttgart.de), O. Sawodny, and C. Tarín are with the Institute for System Dynamics, University of Stuttgart, 70550 Stuttgart, Germany.

978-1-4799-7787-1/15/$31.00 ©2015 IEEE

TABLE I

PARAMETERS.

Symbol	Description	Value	Unit
f_c	carrier frequency	40	kHz
$f_{s,\mathrm{env}}$	envelope sampling freq.	10	kHz
f_{code}	Gold code freq.	500	Hz
T_{chip}	Gold code chip length	2	ms
c_{sound}	speed of sound	343	m/s
λ	ultrasound wave length	≈ 8.575	mm

tilateration algorithm, which is work in progress. The linear distances, which are the measurement results presented in the contribution at hand, are the inputs of this multilateration algorithm, which then yields the position and orientation (six degrees of freedom) of a rigid body.

Tab. I lists some parameters which will be used throughout the paper.

The rest of the paper is organized as follows. Section II gives an overview of the designed positioning system. Section III is devoted to the derivation of the sonar model, including electrical and systemic features. The distance measurement using two different technologies, i. e., ETF and CPH measurements, is described in Section IV. In Section V, relevant experimental results are shown, which are the basis for accuracy estimation. Finally, in Section VI, the main conclusions of the paper are presented and some hints on further work are given.

II. System Overview

In this section, we first describe the overall navigation system, which is currently under development. Then, we describe the isolated task of linear distance measurement, which is dealt with in the present contribution.

A. Navigation System

The overall navigation system that we are developing consists of a mobile unit which is considered to be a rigid body with six degrees of freedom (DOF), as well as at least three receiver units which are located at fixed positions within the room.

The position and orientation of the rigid body is estimated by employing *multilateration*. The individual distances which are used for multilateration are calculated using envelope time-of-flight (ETF) as well as carrier phase (CPH) measurements and are the subject of the present contribution.

The navigation system employs *remote positioning* [14], i. e., the mobile unit transmits signals which are received by several fixed receiver units. The advantage of this approach is that the mobile device can be designed to be small and cheap. Specifically, the mobile device consists of at least three ultrasonic transmitters (US TX) and at least one infrared transmitter (IR TX). This is because we want to resolve not only the position, but also the orientation.

Each fixed measurement unit consists of one ultrasonic receiver (US RX) and an attached infrared receiver (IR RX). It shall be assured that there always exist at least *three line-of-sight links* from the mobile unit to the receiver units.

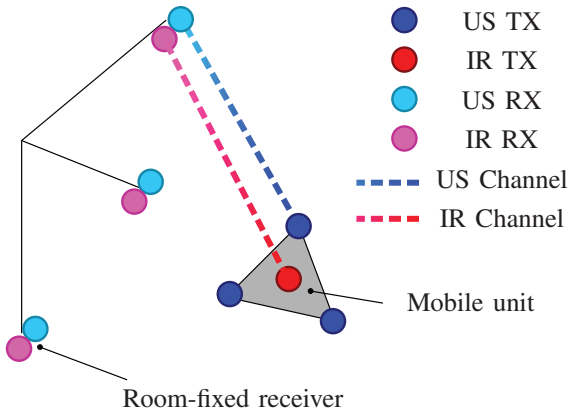

Fig. 1. Schematic navigation system overview: Mobile unit with (at least) three rigidly attached ultrasound transmitters and one infrared transmitter, establishing links to room-fixed measurement units mounted on a frame. Note: only two links are shown.

Each one of those links has *two channels* (ultrasound and infrared). The ultrasound transmitters and receivers are *piezo transducers*, whereas we employ LEDs and photodiodes for the infrared transmitters and receivers, respectively.

Fig. 1 shows the navigation system overview. Please note that – for the sake of clarity – there are only two links (one infrared and one ultrasound) depicted, and not all of them.

The concept of our system is inspired by the global positioning system (GPS), with the main difference that we do not transmit a time reference signal, but instead make use of the two channels with complementary properties: The infrared channel is considered to have no delay, i. e., we approximate the information transmission over the infrared channel to be *instantaneous*. Given the dimensions of the workspace of an indoor navigation system, this approximation seems valid. The ultrasound channel, on the other hand, exhibits a signal propagation velocity equal to the speed of sound c_{sound}.

The kinematic model of the motion unit is described in our previous contributions [15], [16], where we considered the special case of the motion unit being a surgical instrument used in minimally-invasive surgical interventions.

B. Linear Distance Measurement

The basis for multilateration is the measurement of a linear distance. To this end, we consider a testrig consisting of a transmitter printed circuit board (TX PCB), and a receiver (RX PCB). The distance between the TX and RX can be varied. Fig. 2 shows a scheme and a picture of the experimental setup at our institute.

The PCBs are depicted in Fig. 3. Please note that those are not yet miniaturized.

III. Sonar Model

In this section, we derive a simplified electro-mechanical model of the transmitter and receiver, taking into account both the piezos used for ultrasound generation and sensing.

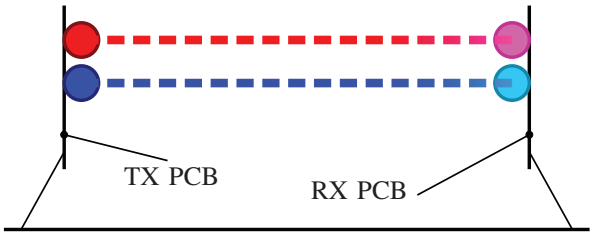

(a)

(b)

Fig. 2. Testrig used for linear distance measurement: (a) Scheme, (b) Experimental setup.

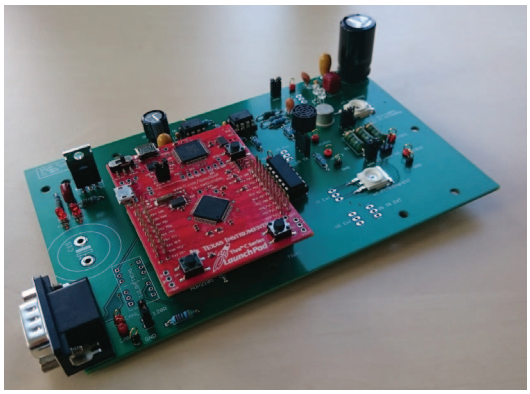

(a)

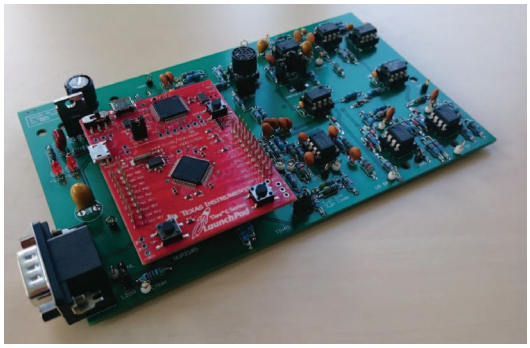

(b)

Fig. 3. Printed circuit boards: (a) TX, (b) RX.

TABLE II

EXPERIMENTALLY IDENTIFIED PIEZO PARAMETERS.

	Symbol	Value	Unit
TX	R_0	31.40	kΩ
TX	C_0	2.01	nF
TX	R_1	33.18	Ω
TX	C_1	282.34	pF
TX	L_1	53.84	mH
RX	R_0	26.70	kΩ
RX	C_0	2.35	nF
RX	R_1	297.97	Ω
RX	C_1	332.78	pF
RX	L_1	51.33	mH

The simulation model is used in the design process of our testrig. It is helpful in the design process of the necessary filters, which are implemented as analog (i. e., continuous-time) filters on a PCB due to the relatively high frequencies involved. Performing filtering operations on the carrier with a digital (and therefore discrete-time) filter in real-time would result in too much data traffic.

The scheme of the transmitter is depicted in Fig. 4: The modulated signal is amplified and drives an ultrasonic piezo transmitter as well as an infrared LED.

The piezo itself can be characterized using its extended electrical equivalent circuit, which is shown in Fig. 5. R_0 and C_0 are actual electrical properties, whereas R_1, C_1, and L_1 are electrical equivalents of the piezo's mechanical properties.

The impedance is given by

$$\begin{aligned} Z_{\mathrm{P,ext}}(s) &= \frac{U_P(s)}{I_P(s)} \\ &= \frac{1}{sC_0} \left|\left| \frac{1}{G_0} \right|\right| \left(R_1 + \frac{1}{sC_1} + sL_1 \right) \\ &= \frac{b_2 s^2 + b_1 s + b_0}{a_3 s^3 + a_2 s^2 + a_1 s + a_0} \end{aligned} \tag{1}$$

with

$$\begin{aligned} &b_2 = C_1 L_1 R_0, b_1 = R_0 R_1 C_1, b_0 = R_0, \\ &a_3 = C_0 C_1 L_1 R_0, a_2 = C_1 (C_0 R_0 R_1 + L_1), \\ &a_1 = R_0 C_0 + R_0 C_1 + R_1 C_1, a_0 = 1. \end{aligned}$$

The parameters of this equivalent circuit are experimentally identified using the method described in [17], [18] on the real piezo transducers (transmitter TX and receiver RX, respectively). This yields values for R_0, C_0, R_1, C_1, and L_1, which are given in Tab. II.

The magnitude plot of the Bode diagram of the piezo impedance is given in Fig. 6, where the experimentally identified parameters are plugged in Eq. (1).

One can clearly see that the resonance of the transmitter overlaps with the antiresonance of the receiver. The carrier frequency f_c is chosen according to the *nominal* transmitting piezo's resonance frequency given in its datasheet as 40 kHz.

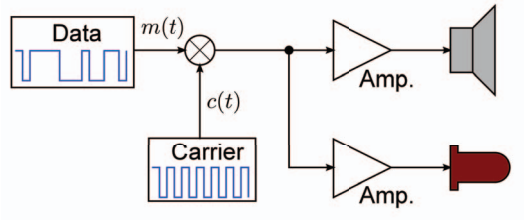

Fig. 4. Scheme of the transmitter: Signal modulation and amplification.

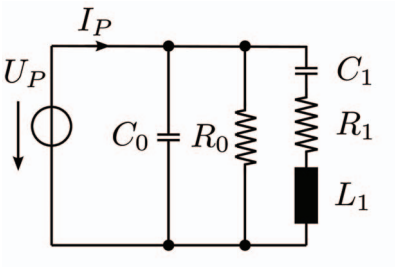

Fig. 5. Extended piezo electrical equivalent circuit.

IV. Distance Measurement

The ETF and CPH distance signals are complementary: The ETF mode yields a *coarse* but *unique* distance signal, whereas the CPH mode yields a *high resolution* but *ambiguous* distance signal. Those signals are similar to the ones encountered in carrier phase GPS.

A. Envelope Time-of-Flight (ETF) Mode

We employ Gold code [19] modulation for the time-of-flight measurement. This is superior to individual ultrasonic "pings" or bursts, because multipath effects are suppressed. Moreover, each transmitting piezo can be assigned a unique code, making it possible for them to share a single carrier frequency using CDMA. The latter feature is especially useful if commercially available piezo transducers are employed, because those are only available for a few individual frequencies. The employed code is depicted in Fig. 8.

We perform a *circular correlation* of the received infrared and ultrasound code with the reference code. This can be written in the form of a *circular convolution*, which in turn can efficiently be evaluated using the FFT algorithm.

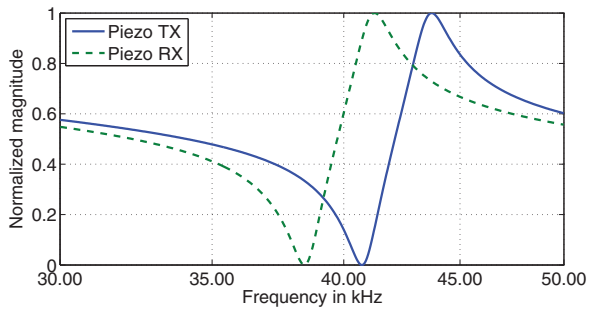

Fig. 6. Magnitude of fitted piezo impedance using experimentally identified parameters of the electrical equivalent circuit.

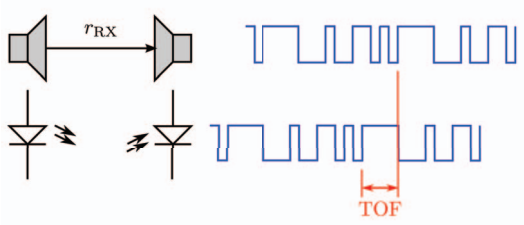

Fig. 7. A two channel link (ultrasound and infrared) is used for the transmission of Gold code modulated signals.

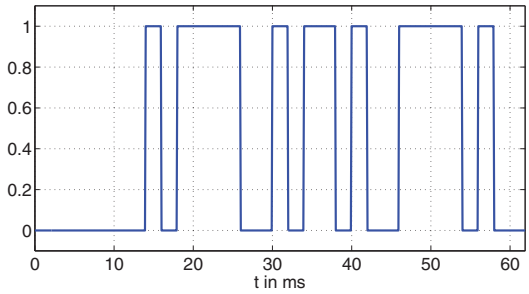

Fig. 8. The actual Gold code which is employed in the experiments.

The circular correlation is defined as

$$\theta[i] = x[i] \times y[i] = \sum_{j=0}^{m-1} x[j]y[(j-i) \bmod m], \qquad (2)$$

whereas (according to [20]) the circular convolution is defined as

$$x[i] \otimes y[i] = \sum_{j=0}^{m-1} x[j]y[(i-j) \bmod m] \qquad (3)$$

and can be efficiently evaluated as

$$x[i] \otimes y[i] = \mathcal{F}^{-1}\left(\mathcal{F}(x[i]) \cdot \mathcal{F}(y[i])\right). \qquad (4)$$

Here, $\mathcal{F}(\cdot)$ denotes the direct DFT and the inverse DFT is written as $\mathcal{F}^{-1}(\cdot)$.

The relation between the circular convolution and the circular correlation is given by

$$\begin{aligned} x[i] \otimes y[i] &= \sum_{j=0}^{m-1} x[j]y[(i-j) \bmod m] \\ &= \sum_{j=0}^{m-1} x[j]\bar{y}[(j-i) \bmod m] = x[i] \times \bar{y}[i] \end{aligned} \qquad (5)$$

with

$$\begin{aligned} &\bar{y}[(j-i) \bmod m] = y[(i-j) \bmod m] \\ &\quad \Leftrightarrow \bar{y}[v \bmod m] = y[-v \bmod m] = y[(m-v) \bmod m]. \end{aligned}$$

The position of the maximum value of the correlation then corresponds to the time of flight between transmitter and receiver.

B. Carrier Phase (CPH) Mode

The difference between the zero-crossings of the ultrasound and infrared carrier signals is used to calculate the phase difference. To this end, we use a trigger which is realized as an interrupt on a microcontroller.

The carrier phase difference Δt_{CPH} is ambiguous with respect to the carrier wavelength λ, but yields a high resolution position signal.

The measured quantity is $\varphi_{\mathrm{CPH}} = (r_{\mathrm{RX}} + r_{\mathrm{offset}}) \bmod \lambda$, where r_{RX} is the distance between transmitter and receiver, and r_{offset} is an unknown offset introduced by the finite dimensions of the ultrasound transducers as well as the signal delay due to the filtering operations.

C. Combination of ETF and CPH measurements

The combination of the ETF and CPH distance measurements shall receive some attention. If the ETF accuracy is better (i. e., smaller) than the wavelength λ, no integer ambiguity arises and the combination can be done straightforward. Otherwise, the integer ambiguity resolution will be done by means of optimization methods and algorithmic development. In particular, we take advantage of the fact that we track a rigid body, which means, e. g., that not all integer values actually yield a valid configuration. This algorithmic development is current work and not part of the contribution at hand.

V. Experimental Results

In this section, we provide some experimental results which are obtained using our testrig. First, we show the performance of the envelope time-of-flight (ETF) mode. After that, we present the high resolution of the carrier phase (CPH) mode.

Please note that the experimental setup does *not* yet allow for a comparison with a ground truth. This error analysis will be done when the linear distance measurement method, which is presented in the paper at hand, is combined with a multilateration algorithm currently under development.

A. ETF Results

In order to assess the performance of the linear distance measurement in ETF mode, we move the transmitter several centimeters towards the receiver, then several centimeters away, and then back to the original position.

An extract of the raw infrared and ultrasound signal envelopes is depicted in Fig. 9. The time shift between the IR and US code can clearly be seen.

Performing the correlation of the received IR and US envelopes with the reference Gold code, searching for the location of the respective maxima and calculating their difference gives the time shift between the IR and US signals. Multiplying the time shift with the speed of sound gives the distance signal, which can be seen in Fig. 10. The resolution is given by

$$\Delta s_{\mathrm{ETF}} = \frac{c_{\mathrm{sound}}}{f_s} \approx 3.4\,\mathrm{cm}. \tag{6}$$

and results in quantization noise, which can be seen in the step-like shape of the curve in Fig. 10.

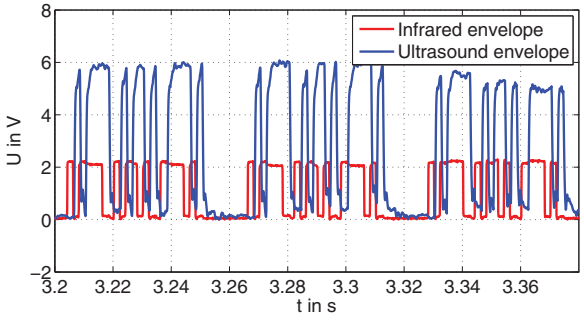

Fig. 9. Extract of the raw infrared and ultrasound signal envelopes.

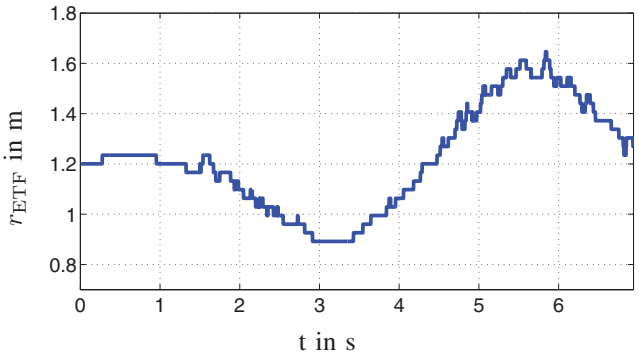

Fig. 10. Results of the ETF mode: Coarse but unique distance signal.

B. CPH Results

For the assessment of the CPH mode, we want a small displacement between TX and RX in order to show the high resolution. This can be achieved by manually pushing against a corner of the PCB on which the transmitter is mounted. This induces a bending of the PCB and therefore a small displacement in the millimeter range. The large movement of the ETF experiment is not suited here. However, when combining the ETF and CPH results in the framework of multilateration, both signals describe the same movement.

The CPH results are depicted in Fig. 11. During the first two seconds, no bending was induced (yellow region). The slight deviation of the phase from a horizontal line can be explained by temperature variations, which in turn change the speed of sound. A change of one degree Celcius in room temperature results in a distance measurement deviation of approx. $2\,\mathrm{mm}$. As those temperature changes apply to all sonar links, they can be compensated in the multilateration process. In the last two seconds (magenta region), the sine shaped displacement due to bending can clearly be seen. Please note the high resolution of the system in the submillimeter range, which results in a very smooth curve.

VI. Conclusion and Further Work

We developed a system for linear distance measurement combining and ultrasound and infrared channel together with spread spectrum techniques and carrier phase measurement.

A large part of the work was dedicated to the development of an accurate simulation model of the devices involved,

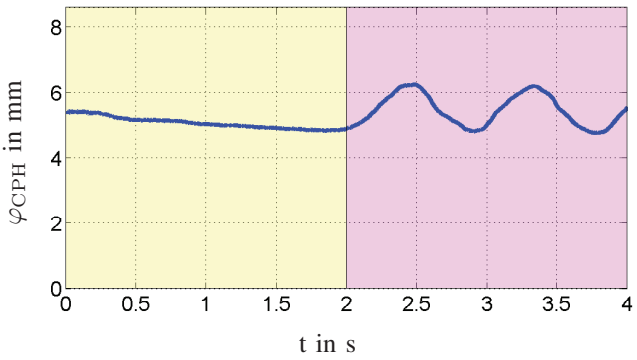

Fig. 11. Results of the CPH mode: Bending of the PCB begins after two seconds, resolution in submillimeter range.

especially the ultrasound transducers. The parameters of the model were identified experimentally, so that the model could be used in the system design.

We provided experimental results on a testrig which show the good performance of both the ETF as well as the CPH mode, providing a corresponding and complementary pair of signals: one coarse but unique, and one high resolution but ambiguous signal.

Current and further work is dedicated to the implementation and experimental test of the multilateration algorithm, which takes as input the linear distances obtained with the system presented in the contribution at hand. Furthermore, the PCBs are subject to miniaturization, so that they can be attached to a rigid body which is to be tracked.

REFERENCES

[1] R. Mautz and S. Tilch, "Survey of Optical Indoor Positioning Systems," in *International Conference on Indoor Positioning and Indoor Navigation (IPIN)*, 2011.

[2] NaturalPoint, Inc., "OptiTrack Motion Capture System." [Online]. Available: http://www.naturalpoint.com/optitrack/

[3] AXIOS 3D Services GmbH, "CamBar." [Online]. Available: http://www.axios3d.de/

[4] S. Dayekh, S. Affes, N. Kandil, and C. Nerguizian, "Cooperative Localization in Mines Using Fingerprinting and Neural Networks," in *IEEE Wireless Communications and Networking conference (WCNC)*, 2010.

[5] Y. Jin, W.-S. Soh, and W.-C. Wong, "Indoor Localization with Channel Impulse Response Based Fingerprint and Nonparametric Regression," *IEEE Trans. on Wireless Cmmunications*, vol. 9, pp. 1120–1127, 2010.

[6] H.-H. Lin, C.-C. Tsai, and J.-C. Hsu, "Ultrasonic Localization and Pose Tracking of an Autonomous Mobile Robot via Fuzzy Adaptive Extended Information Filtering," *IEEE Trans. Instrum. Meas.*, vol. 57, no. 9, pp. 2024–2034, 2008.

[7] S. J. Kim and B. K. Kim, "Accurate hybrid global self-localization algorithm for indoor mobile robots with two-dimensional isotropic ultrasonic receivers," *IEEE Trans. Instrum. Meas.*, vol. 60, pp. 3391–3404, 2011.

[8] S. Kim and B. Kim, "Dynamic Ultrasonic Hybrid Localization System for Indoor Mobile Robots," *IEEE Transactions on Industrial Electronics*, vol. 60, pp. 4562–4573, 2013.

[9] N. B. Priyantha, "The Cricket Indoor Location System," Ph.D. dissertation, Massachusetts Institute of Technology, 2005.

[10] J. Prieto, A. Jimnez, J. Guevara, J. Ealo, F. Seco, J. Roa, and F. Ramos, "Performance Evaluation of 3D-LOCUS Advanced Acoustic LPS," *IEEE Trans. Instrum. Meas.*, vol. 58, pp. 2385–2395, 2009.

[11] N. Aloui, K. Raoof, A. Bouallegue, S. Letourneur, and S. Zaibi, "Performance evaluation of an acoustic indoor localization system based on a fingerprinting technique," *EURASIP Journal on Advances in Signal Processing*, vol. 13, 2014.

[12] I. Rishabh, D. Kimber, and J. Adcock, "Indoor localization using controlled ambient sounds," in *International Conference on Indoor Positioning and Indoor Navigation*, 2012.

[13] Y. Itagaki, A. Suzuki, and T. Iyota, "Indoor Positioning for Moving Objects Using a Hardware Device with Spread Spectrum Ultrasonic Waves," in *International Conference on Indoor Positioning and Indoor Navigation*, 2012.

[14] M. Vossiek, L. Wiebking, P. Gulden, J. Wieghardt, C. Hoffmann, and P. Heide, "Wireless Local Positioning," *IEEE Microwave Magazine*, vol. 4, pp. 77–86, 2003.

[15] P. Rapp, L. Hägele, O. Sawodny, and C. Tarín, "Performance Study for an Acoustic-Inertial Close Range Navigation System used in Minimally-Invasive Surgical Interventions," in *Proceedings of the European Control Conference*, 2014.

[16] ——, "Characterization of a 6 DOF Acoustic-Inertial Navigation System for Minimally-Invasive Surgery," in *Proceedings of the International Conference on Control, Automation, Robotics and Vision (ICARCV)*, 2014.

[17] *Standard Definitions and Methods of Measurement for PIEZOELECTRIC VIBRATORS*, IEEE Std. 177, May 1966.

[18] W. L. Smith, *Ultrasonic Measurement Methods*, 1st ed., ser. Physical Acoustics. Academic Press, 1990, vol. 19, ch. 6: Measuring the Electrical Characteristics of Piezoelectric Devices, pp. 267–290. [Online]. Available: http://www.sciencedirect.com/science/bookseries/0893388X/19

[19] R. Gold, "Optimal Binary Sequences for Spread Spectrum Multiplexing," *IEEE Trans. on Information Theory*, vol. 13, pp. 619–621, 1967.

[20] A. V. Oppenheim, R. W. Schafer, and J. R. Buck, *Discrete-Time Signal Processing*. Prentice Hall, 1999.